


Article

Medial Opening Wedge High Tibial Osteotomy in Knee Osteoarthritis—A Biomechanical Approach

Nicolae Florin Cofaru ¹, Mihai Dan Roman ², Ileana Ioana Cofaru ³, Valentin Stefan Oleksik ^{4,*} 
and Sorin Radu Fleaca ² 

¹ Department of Industrial Engineering and Management, Faculty of Engineering, “Lucian Blaga” University, 550024 Sibiu, Romania; nicolae.cofaru@ulbsibiu.ro

² Department of Orthopedics and Traumatology, Faculty of Medicine, “Lucian Blaga” University, 550024 Sibiu, Romania; mihai.roman@ulbsibiu.ro (M.D.R.); radu.fleaca@ulbsibiu.ro (S.R.F.)

³ Department of Computer Science and Electrical Engineering, Faculty of Engineering, “Lucian Blaga” University, 550024 Sibiu, Romania; ioana.cofaru@ulbsibiu.ro

⁴ Department of Industrial Machines and Equipment, Faculty of Engineering, “Lucian Blaga” University, 550024 Sibiu, Romania

* Correspondence: valentin.oleksik@ulbsibiu.ro

Received: 22 November 2020; Accepted: 14 December 2020; Published: 16 December 2020



Featured Application: This research provides a “mini intraoperative guide” for geometrical and dimensional planning of the medial wedge open high tibial osteotomy. The values obtained in our study are useful for preventing or minimizing the microfractures that can occur in the center of the rotation of the angulation (CORA) hinge area.

Abstract: This paper provides an analysis from a biomechanical perspective of the medial opening wedge high tibial osteotomy surgery, a medical procedure commonly used in treating knee osteoarthritis. The aim of this research is to improve the analysed surgical strategy by establishing optimal values for several very important parameters for the geometric planning of this type of surgical intervention. The research methods used are numerical and experimental. We used finite element, a numerical method used to study the intraoperative behavior of the CORA area for different positions of the initiation point of the cut of the osteotomy plane and for different correction angles. We also used an experimental method in order to determine the maximum force which causes the occurrence of cracks or microcracks in the CORA area. This helped us to determine the stresses, the maximum forces, and the force-displacement variations in the hinge area, elements that allowed us to identify the optimal geometric parameters for planning the surgery.

Keywords: medial opening wedge high tibial osteotomy; correction angle; osteotomy cutting point; finite element method (FEM) analysis; CORA point

1. Introduction

Knee osteoarthritis is a fairly common condition today and is characterized by the progressive wear of the articular cartilage and the degradation of the knee joint [1–4]. The disease predominantly affects women and usually occurs in people aged over 40 [1,5–8].

The main factors involved in knee osteoarthritis aethiology are mechanical and inflammatory. Mechanical factors generate an increase of focal pressure on cartilage, while inflammatory conditions determine a decrease of cartilage mechanical strength [1,9]. Any of these conditions lead to an overstress and, as a consequence, to the rupture of the cartilage tissue. Mechanical factors may be intraarticular, such as fractures consolidated with chondral surface step-offs, and meniscal lesions, traumatic chondral

lesions, or extraarticular, such as axial deviations of the limb in the frontal or the sagittal plane [10]. Frequently, the cartilage damage, usually involving initially one knee compartment (medial or lateral), generates axial deviations of the limb, generating a positive feed-back loop, which leads to an increase in focal pressure on the already damaged articular cartilage [11].

One of the common situations that can occur in the above described scenarios is medial knee osteoarthritis with varus knee. An important biomechanical effect of this condition is the increase of the load in the knee joint. Hence, if on a healthy knee, the maximum forces acting on the knee during gait can reach up to three times the body weight, there are studies [12,13] showing that a deviation angle of only 10 degrees varus causes a stress on the medial compartment of up to 7.4 times body weight and a fourfold increase of the risk of ingravescence of the medial osteoarthritis.

The medial opening wedge high tibial osteotomy (hereinafter, “medial opening wedge HTO”) is one of the procedures used to treat this condition. This is a surgical procedure used especially in the case of young adults with unicompartmental knee osteoarthritis that restores or even overcorrects the mechanical limb axis, immediately improving the knee function, conferring a long time cartilage protection, and relieving the pain [12,14–18].

The main purpose of this research is to optimize the operative technique for treating knee osteoarthritis and for correcting the related axial deviations through medial opening wedge HTO.

In order to highlight the geometrical parameters that are studied in our research, Figure 1 shows the geometric planning of the surgical intervention using one of the most frequently used methods in this sense, i.e., the Miniaci method [19,20].

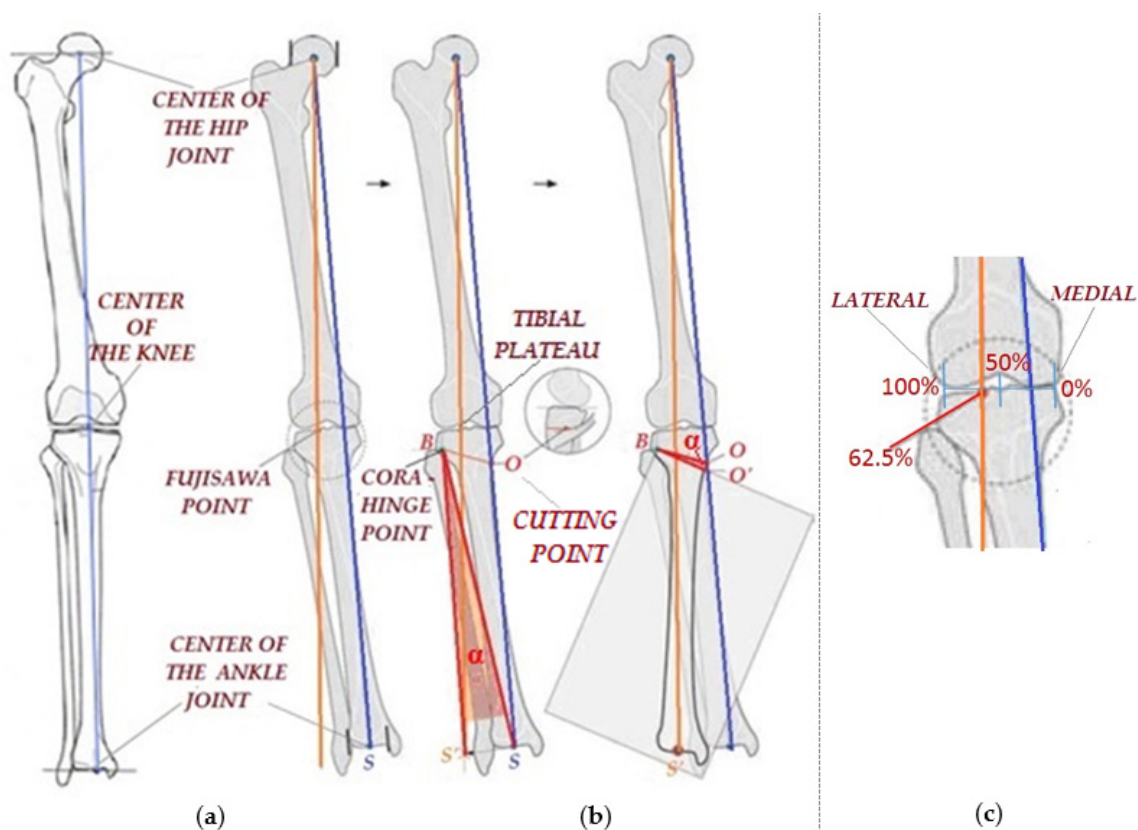


Figure 1. Medial open wedge high tibial osteotomy (HTO)—mechanical axis of the lower limb (a), main steps (b) and Fujisawa point (c).

Figure 1a shows the the mechanical axis of the lower limb in the case of a healthy knee. As can be observed, this axis passes through the center of the femoral head through the middle of the knee and through the center of the ankle joint.

As shown in Figure 1b, in the case of a patient with knee osteoarthritis, this axis does not pass through the middle of the knee but intersects the medial compartment, overstressing it. The purpose of the medial opening wedge HTO is that of correcting the axial deviation, i.e., of bringing the mechanical axis back to the correct position.

The main steps for correcting the axial deviation using the Miniaci method [19,20] are the following:

- Draw a line (orange) that passes through the center of the femoral head and through a point known in the scientific literature as the “FUJISAWA point” (Figure 1b) [19,21–23]. As can be observed from Figure 1b,c the Fujisawa point is a point positioned at 62.5% on the medial to lateral transverse knee line (hereinafter, “the FUJISAWA point”). The precise positioning of this point is still a controversial topic among specialists. It should normally be positioned halfway between the medial compartment and the lateral part (Figure 1c), but due to the predisposition of the affected patient to a continuous wear of the intra-articular cartilage, an overcorrection is preferred in the sense that the point is positioned at 62.5% of the distance. There is also the possibility that the surgeon chooses to set this point between 50 and 70%, depending on the degree of cartilage wear [21].
- Determine the position of the “hinge” point B relative to the tibial plateau and to the lateral cortex of the tibia (Figure 1b). This is the point around which the angulation is made, i.e., the center of the rotation of the angulation (hereinafter, “CORA”). This point is important because one needs a stable lateral hinge, and a fracture line through the articular surface should be avoided. There are no specifically defined values on this matter in the operative technique, but rather ranges of values are taken into consideration: 15–20 mm relative to the articular plane and 5–10 mm relative to the lateral cortex of the tibia [20,24–26].
- Afterwards, the point of initiation of the cut for performing the osteotomy, situated on the medial cortex, is established (depicted as “point O” in Figure 1b, hereinafter “cutting point”). There are no studies suggesting the accurate positioning of the cutting point. However, given the limitations generated by the surrounding anatomic structures, the cutting point should be placed at a minimum of 30 mm and at a maximum of 50–60 mm from the articular line [20,24–28]. The osteotomy line is depicted as BO line in Figure 1b.
- Further on, the opening correction angle α is determined (hereinafter, “correction angle”) (Figure 1b). For this, a line is drawn from point B to point S, the center of the ankle joint, and then a circular arc is drawn with the center in point B of radius BS from point S to the intersection with the previously drawn orange line, resulting in point S'. Angle α , formed between line BS and line BS', is the correction angle. The line joining the center of the femoral head and point S' is the new corrected mechanical axis. To actually obtain the correction, a wedge osteotomy (depicted as “OBO” in Figure 1b) is performed, having at its tip the angle α , which displaces the mechanical axis to the desired position. The 3D rotation of the proximal fragment of the tibia around the hinge is presented in Section 2.

From the geometric parameters presented in the above, we further focus our attention on the following (depicted also in Figure 1b):

- The correction angle.
- The position of the cutting point relative to the corresponding tibial plateau.

The behaviour of the bone at the CORA point can generate fracture lines to the articular surface of the lateral plateau and can also generate fracture lines to the lateral cortex of the proximal tibia [29]. An important issue regarding this point is that it should allow the opening of the osteotomy, but it should not generate instability that would finally lead to a non-union of the osteotomy gap. There are few objective data in the literature that analyze the influence of the correction angle and of the positioning of the cutting point on the mechanical behaviour of the bone around the CORA point.

The working hypothesis in our research is that the positions of the cutting point and the correction angle are influencing the mechanical properties of the lateral hinge. The final aim of this study is to

determine the optimal positioning of the cutting point relative to the correction angle α by analyzing the mechanical behaviour of the lateral hinge.

The objectives of the research are the following:

- To conduct a numerical research using the finite element method (hereinafter, “FEM”) to study the intraoperative behavior of the CORA area for different positions of the cutting point and for different correction angles. The FEM analysis may predict the mechanical stresses developed at the lateral hinge and the risk of fracture.
- To conduct a similar experiment on mechanical loading behavior.

Specifically, this paper focuses on providing a “mini intraoperative guide” for geometrical and dimensional planning of the medial wedge open HTO, with the aid of which surgeons can choose the best values for the studied geometrical parameters, i.e., the position of the cutting point and the correction angle, so as to avoid or minimize the risk of microfractures that could occur in the CORA area.

2. Materials and Methods

To achieve the previously mentioned objectives, the main research methods applied are 3D computer aided design (hereinafter, “CAD”) modelling, computer aided engineering (hereinafter, “CAE”) simulations, and analyses using the finite element method or the experimental method.

2.1. The Numerical Simulation of the Uniplane Opening Tibial Osteotomy

A first stage of the research is the numerical simulation by the finite element method and consists of some static analyses of the CORA area. The behavior of this area is very important because the occurrence of micro-cracks or cracks in the CORA area can have consequences on both the smooth conduct of the surgery and on a good subsequent recovery.

The software used to perform the analyses is Ansys.

The purpose of the performed static analyses is to determine the state of stresses in the CORA area for the uniplane opening osteotomies, taking into account the studied parameters, namely: X_1 —the position of the cutting point relative to the corresponding tibial plateau (Figure 2a) and X_2 —the value of the required correction angle (Figure 2b).

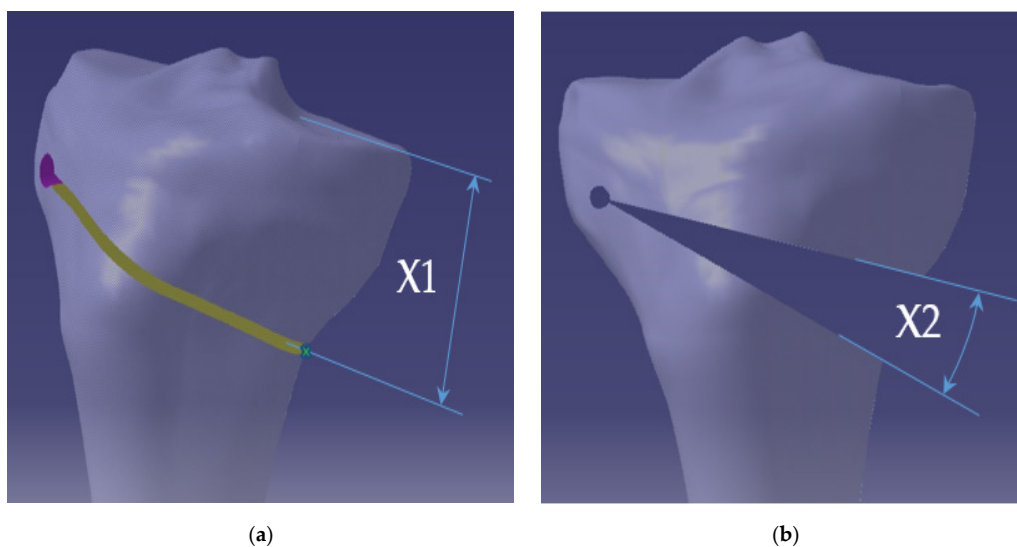


Figure 2. Analyzed geometric parameters: (a) position of the cutting point; (b) the value of the correction angle.

The characteristics of the materials necessary for performing these analyses resulted from the previously conducted bibliographic study [30–40]. The values for the healthy mature bone, as summarized in [41], are the following:

- Young's modulus (E)—12 to 19 GPa for the cortical bone, 0.5 to 1.5 GPa for the spongy bone, and 0.01 to 0.015 GPa for the articular cartilage.
- Poisson's ratio—0.3 to 0.35 for the cortical bone, 0.16 to 0.2 for the spongy bone, and 0.2 to 0.25 for the cartilage.
- Transverse modulus of elasticity (G)—4 to 7 GPa for the cortical bone.
- Fracture resistance (Rm)—115 to 125 MPa for the cortical bone.
- Elongation (A)—1.4 to 2.8% for the cortical bone.
- Porosity—5 to 10% for the cortical bone, 50 to 90% for the trabecular bone.
- Density—1.6 to 1.9 g/cm³ for the cortical bone, 0.2 to 1 g/cm³ for the trabecular bone.

Considering that the opening osteotomies are made in the epiphyseal tibial area, mainly characterized by spongy bone, the use of the following mechanical characteristics in the FEM analyses was agreed upon: Young's modulus—1000 MPa, Poisson's ratio—0.18.

In order to ensure the intraindividual variability of the simulations, we note that, in our calculation, we used the elastic modulus, taking into account the dependency relation between the bone's density and the elastic modulus. It is already known that researchers use a high variety of dependency relations between the bone density and the elastic modulus (linear laws, exponential laws). Out of these, we considered: $E = C \cdot \rho^\beta$, where E is the elastic modulus, C is a coefficient, and β is an exponent whose value varies in accordance to the nature of the bone (cortical or trabecular). Namely, the dependency function used was $E = 8.92 \cdot \rho^{1.83}$ [42] for a trabecular bone subjected to a compression load. By doing so, we could estimate what the maximum value of the loads in the bone component was by simply modifying the value of the elastic modulus.

The starting point for obtaining the geometrical models was a 3D model of a human tibia, a component of a professional model of a human inferior leg. The model was acquired from the ZYGOTE company, a world leader in 3D anatomic modelling.

Afterwards, the modelling of the medial open wedge HTO surgery was achieved by using the Catia V5R20 software. As we sought to obtain a CAD-CAE system with a high degree of generality and applicability, the models were achieved through a parametrized and generalized modelling. In this sense, the main variables that control, from a geometric and a dimensional point of view, the surgery were defined as parameters in the 3D modelling. By doing so, a mere modification of the parameters' values allowed us to obtain the desired geometrical model.

For creating this models, we took into account the steps and the geometric elements that are used in the actual surgery.

The relevant elements were positioned on the tibial model (Figure 3a): CORA axis, medial cortex, and the cutting point. We note that, during the modelling, the cutting point was constrained so as to permanently coincide with the medial cortex and so its position can be defined relative to the tibial plateau (30, 40, 50 mm in our study). Additionally, we note that the line (depicted in blue in Figure 3a) that started from the cutting point and was perpendicular on the CORA axis defined, together with the CORA axis, the osteotomy plane.

To achieve the correction, it was necessary to rotate the proximal segment of the tibia around the CORA axis (Figure 3b). The correction angle was measured between the successive positions (before and after the rotation) of the blue line (depicted in Figure 3c) that started from the cutting point and was perpendicular on the CORA axis (Figure 3c).

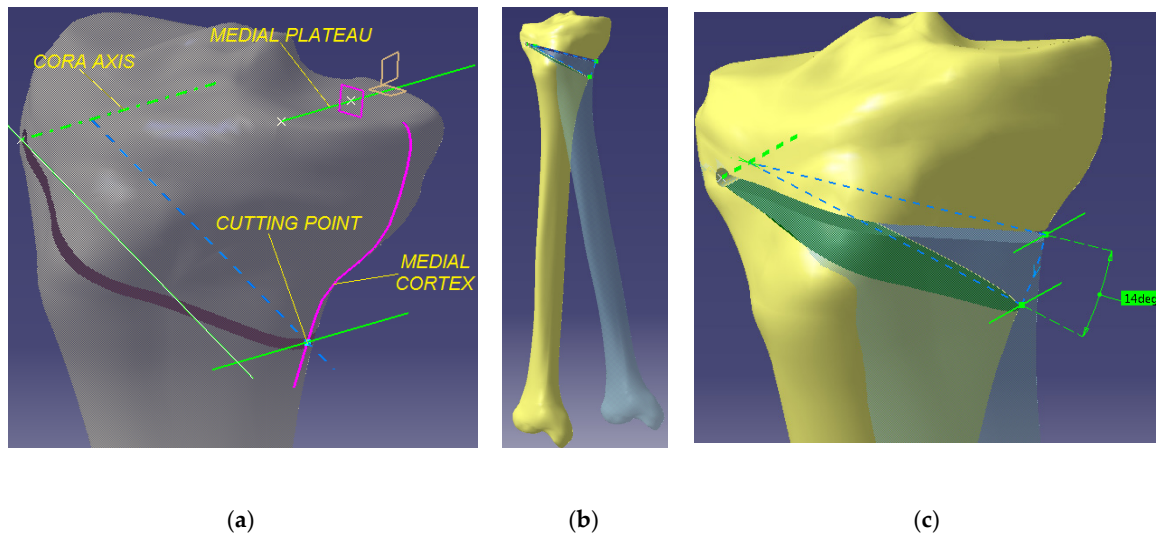


Figure 3. 3D modelling of the medial open wedge HTO surgery: (a) geometrical elements; (b) 3D rotation; (c) correction angle.

In this way, we obtained the geometrical models that were necessary for the FEM analyses, models that were later imported in the ANSYS software. These are differentiated by parameters X_1 and X_2 , to which the values listed in the table below were assigned (Table 1):

Table 1. Values assigned to the variables and their combinations.

| No. | X_1 (mm) | X_2 (degree) |
|-----|------------|----------------|
| 1 | 30 | 6 |
| 2 | 30 | 10 |
| 3 | 30 | 14 |
| 4 | 40 | 6 |
| 5 | 40 | 10 |
| 6 | 40 | 14 |
| 7 | 50 | 6 |
| 8 | 50 | 10 |
| 9 | 50 | 14 |

The values assigned to variable X_1 were justified by the data collected from scientific literature [20,24–28], which proves that, as mentioned above, this distance should not have been smaller than 30 mm, nor should it have exceeded 50 to 60 mm. Obviously, the anatomical dimensions of the bone were also taken into consideration. Consequently, the values chosen for the FEM analyzes were: 30, 40, and 50 mm.

The second variable, X_2 , was the angle at the tip of the osteotomy wedge, which was identical to the correction angle. The variable was important because the higher the correction angle was, the higher the probability of CORA area cracking was. Possible correction angles resulting from literature [20,24–28] and surgical practice ranged between 4–5 degrees to 16–18 degrees. The boundaries were given by the fact that a value that was too low did not justify the surgery, and a value that was too high made the surgery impossible.

Consequently, the values considered appropriate for this research were: 6, 10, and 14 degrees. As shown in Table 1, all possible combinations between the values of the two variables were considered, thus resulting in nine geometric CAD models.

With respect to the degree of precision of the analyses performed by using the finite element method, we note that the network of used elements (a network of tetrahedric elements) was generated so the element size did not exceed 1 mm. Hence, the meshed model contained 861,371 finite elements

connected one to another through 1,261,857 nodes. Moreover, the check mesh quality function was activated, and a 100% obsolete mesh percentage resulted. By doing so and by performing a slow type transition from the large size elements to those of a reduced size, we made sure that the error percentage did not exceed 3%, a unanimously accepted value in the scientific community.

Figure 4a shows the model meshed for a cutting point located at 30 mm from the tibial plateau and a correction angle of 14 degrees. The method of applying the necessary stresses and constraints on the model (Figure 4b) considers the angular removal of the two sides of the osteotomy cut in order to achieve the osteotomy wedge at the desired correction angle. In this regard, a fixed constraint was considered, located on the side facing the joint, while the other face was subjected to a uniformly distributed stress.

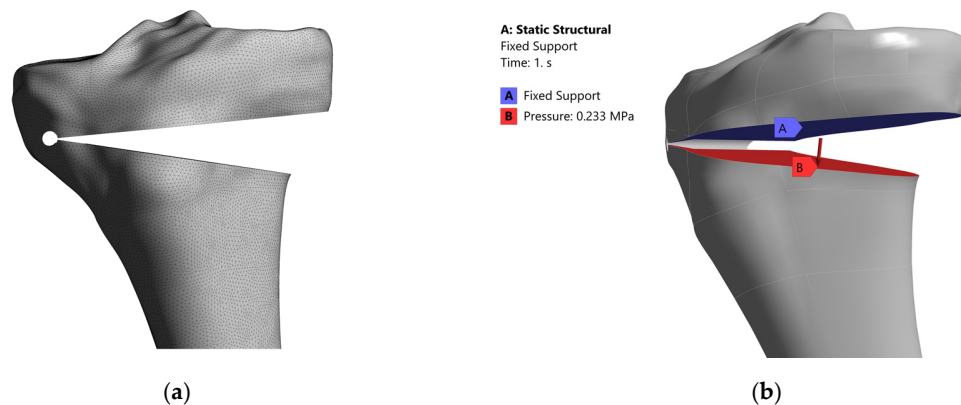


Figure 4. (a) Meshing the model and (b) application of stresses and constraints.

The static structural analysis was made when the required correction angle was reached. It should be noted that the pressure applied on the lower face of the osteotomy was obtained by relating the value of the applied force to the surface on which it was distributed.

The value of this force depended on the size of the correction angle. Literature [24,43] and previous surgical experiences suggest considering the following values: 75 N for the 6 degree angle, 150 N for the 10 degree angle, and 250 N for the 14 degree angle. The values of the surfaces on which it acted resulted from using the facilities provided by the Ansys software.

After running the numerical simulations, the von Mises stresses and the maximum principal stresses were determined.

2.2. Experimental Research on the Study of the Intraoperative Behavior of the Bone Structure in the Case of the Opening Tibial Osteotomies

This subchapter covers an experimental approach to the issues covered in the previous subchapter.

The aim of the investigation is to study, experimentally this time, the CORA area, by determining the maximum force— F_{\max} (N)—which causes the occurrence of cracks or microcracks as well as the variation of force F (N) in relation to the strain required for performing the osteotomy wedge.

The input variables were the same as those taken into account in the previous numerical study, namely: X_1 —the position of the cutting point relative to the corresponding tibial plateau (Figure 2a) and X_2 —the value of the required correction angle (Figure 2b). The values of these variables and their combinations are also identical to those presented in Tables 1 and 2, thus resulting in nine distinct experiments.

The specimens on which the experimental tests were performed were properly prepared bovine tibias taken on the day the animals were slaughtered. We opted for this type of bones because the bovine knee has many similarities with the human knee regarding bone structure (cortical and spongy bone), bone anatomy, meniscus, ligaments (both cruciate and collaterals), and extensor mechanism. As a result of this, as far as mechanical loading is concerned, the bovine bones behave

similarly to the human bones. The ovine and the swine knees, which are also similar to the human knee (considering the properties described), are smaller in dimensions and hence more susceptible to generating experimental errors. Two of the three tibias were collected from the same cow, and the third came from a cow originating from the same family.

Table 2. The values of the stresses resulted from the finite element method (FEM) analyses.

| No. | X ₁ (mm) | X ₂ (Degree) | Von Mises Stress (MPa) | Max. Principal Stress (MPa) |
|-----|---------------------|-------------------------|------------------------|-----------------------------|
| 1 | 30 | 6 | 67.195 | 76.905 |
| 2 | 30 | 10 | 119.25 | 136.775 |
| 3 | 30 | 14 | 196.61 | 225.49 |
| 4 | 40 | 6 | 65.23 | 74.615 |
| 5 | 40 | 10 | 120.67 | 137.465 |
| 6 | 40 | 14 | 191.65 | 223.865 |
| 7 | 50 | 6 | 69.085 | 78.125 |
| 8 | 50 | 10 | 127.73 | 145.755 |
| 9 | 50 | 14 | 198.16 | 230.905 |

Using appropriate surgical instruments, the soft structures (muscles, patellar tendon, patella, collateral and cruciate ligaments (anterior and posterior), and menisci) were removed, resulting in a clean proximal bovine tibia. Both the cleaning of the tibias and the actual performance of the cuts for the osteotomy were conducted by the orthopedic surgeons who co-authored this article, in accordance with the surgical protocols they use for real surgeries.

Thus, the position of the CORA point was established, followed by its actual materialization, by making an anterior and a posterior bore (Figure 5a).

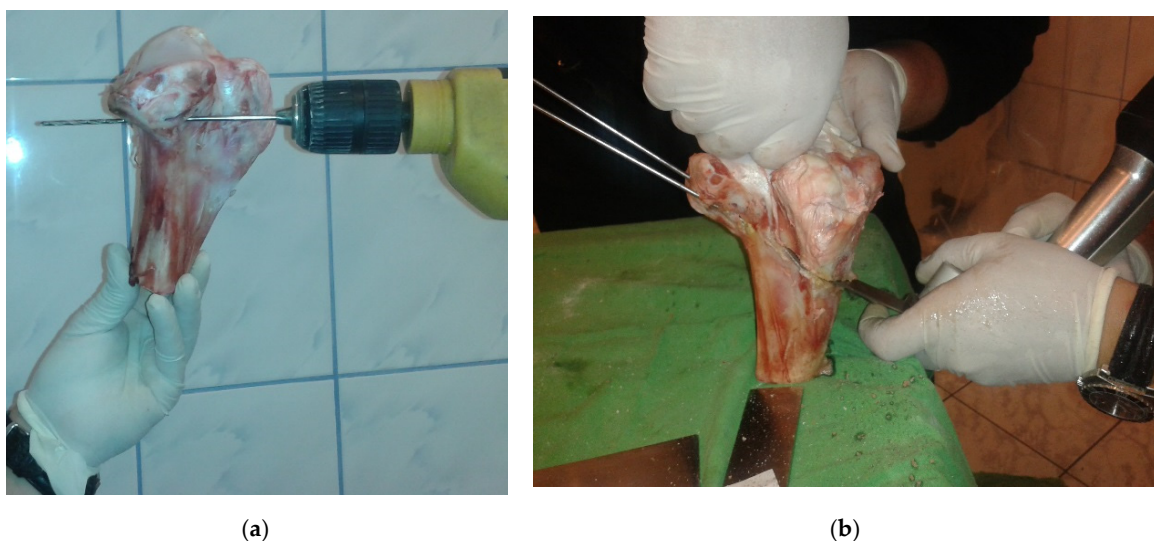


Figure 5. Execution of the hole in center of the rotation of the angulation (CORA) (a) and sectioning the osteotomy plane (b).

After marking the position of the cutting point, two Kirschner pins were used, which, after being properly inserted into the bone structure, served as a guide in sectioning the osteotomy plane (Figure 5b).

The tibial specimens were sectioned similarly at the established distances relative to the tibial plateau: 30 mm, 40 mm, and 50 mm. A graduated prismatic spacer was used to materialize the other variable, namely the correction angle.

Regarding the order in which the information was collected, this was established by taking into account the preservation of the adjustments of the tibial part in relation to the loading device and, at the same time, by seeking to obtain as few assemblies–disassemblies of the tibial part as possible.

Therefore, the nine experimental determinations (corresponding to all the combinations of the values of the variables) were made by successively fixing three tibias at distances of 30, 40, and 50 mm to the tibial plateau with the correction angles of 6, 10, and 14 degrees, sequentially achieved for each tibia by introducing the spacer in the tibia in a controlled manner.

The experimental stand used was specially designed and executed modularly for the generalized study of the HTO. In this regard, the functions that the stand must fulfill were taken into account during the design phase: orientation and fixation of the tibia, actual execution of the osteotomy wedge at the desired correction angle, control of the position of the contact surfaces and of the application of forces, and adjustment of the position of the tibia.

Since the design of the stand was described in detail in [41], only the important elements are pointed out here (Figure 6a,b). Thus, the orientation and the fastening of the tibia were achieved in a device with self-centering clamping, and its position was ensured by two U-shaped frames providing the possibility to adjust the angle up to 120° in each direction. For the performance of the osteotomy wedge, a graduated prismatic spacer was used, which allowed us to permanently evaluate the achieved correction angle.

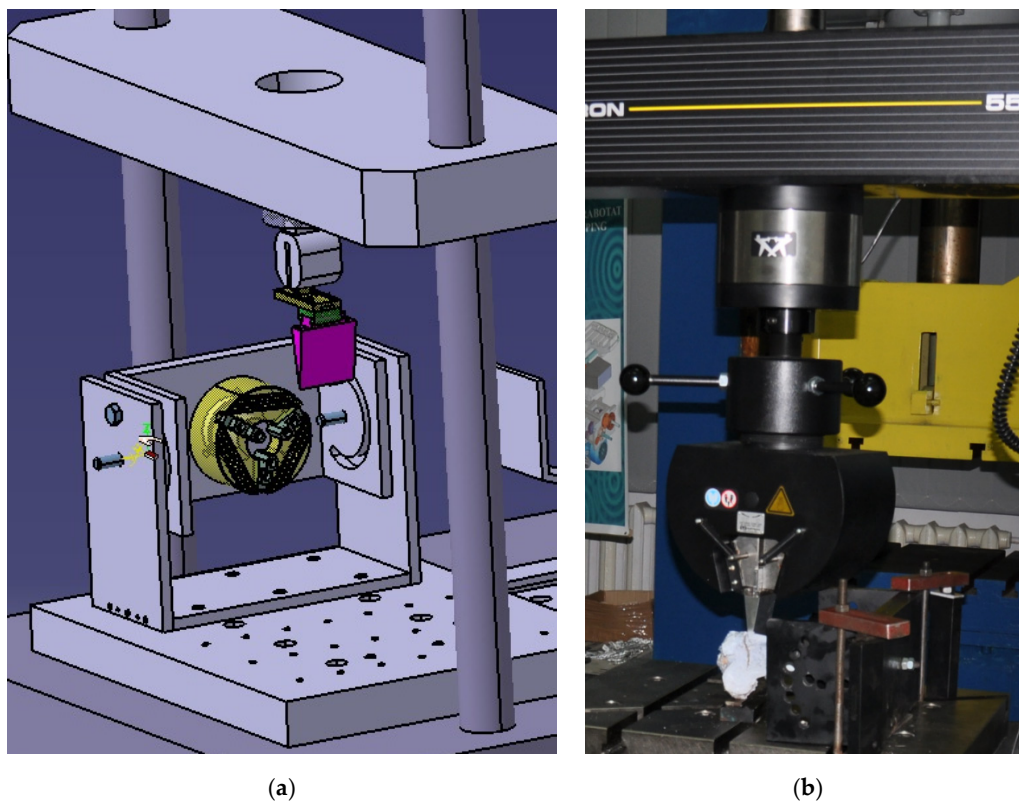


Figure 6. Opening wedge HTO experimental stand: designed and modelled (a) and executed and prepared for the experiment (b).

This specialized stand was mounted on the universal traction, compression, and buckling testing machine Instron 5587. It has a maximum load capacity of 300 kN and is controlled by hardware and software via the digital signal processor (DSP) interface and the Bluehill 2.0 specialized software.

This universal testing tool facilitated the control of the speed of the mobile crosshead to an accuracy of 0.5% and the recording of the force with a precision corresponding to class ASTM E-4 or DIN 51221 Class 1 (standard that describes the procedures for the force verification for static or quasi-static for testing machine). The speed of the mobile crosshead ranged from 0.001 to 500 mm/min. The surface of the machine's fixed plate was 1403×851 mm.

The lower subassembly of the stand where the tibia was fastened was attached to the plate of the machine, while the upper subassembly in which the spacer was mounted was attached to the mobile crosshead, which underwent the relative displacement and the effective load.

Figure 7 shows a detailed image of the stand with the prismatic spacer 1 inserted into the tibia 2 fixed in the self-centering device 3. The “U” type frame 4 ensured the correct orientation of the tibia relative to the prismatic spacer.

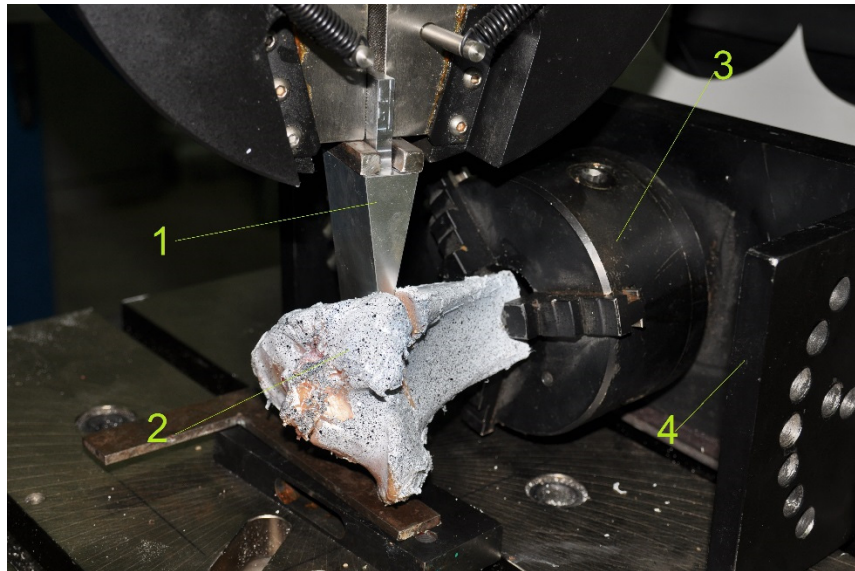


Figure 7. Experimental conduct of medial opening wedge HTO.

In order to materialize the values established for variable X_2 —correction angle—the mobile crosshead of the testing machine performed the necessary displacements in accordance with the gradations marked on the prismatic spacer. These displacements were: 5 mm for the 6 degree angle, 9 mm for the 10 degree angle, and 12 mm for the 14 degree angle.

The experimental results are presented in the next chapter.

3. Results

In this chapter, we present the results of the performed simulations and of the experiments.

3.1. The Results of the Numerical Simulation of the Uniplane Opening Tibial Osteotomy

The analysis of the results obtained from the numerical simulations relates to the maximal values and to the distribution of the von Mises stresses and of the main stresses obtained, with the purpose of evaluating the two studied parameters (the position of the cutting point and the correction angle) in order to optimally plan, from a geometrical and a dimensional point of view, the surgery. Figure 8a,b shows the distributions of the von Mises stresses in the CORA area, both on the inner and on the outer surface of the bone, for the scenario in which the cutting point was situated at a 30 mm distance to the tibial plateau, and there was a 14 degree correction angle.

When observing the results of the analysis, one can notice a maximum equivalent stress on the outer wall of the tibia (Figure 8b) reaching 137.74 MPa, a reasonable value considering the large value of the correction angle (14 degrees). Regarding the state of the equivalent von Mises stresses inside the CORA hole (Figure 8a), high values of the stresses were observed, reaching a maximum of 196.7 MPa, values that could lead to the appearance of microcracks. The maximum principal stresses had higher values, with a maximum of 225.59 MPa achieved inside the CORA area.

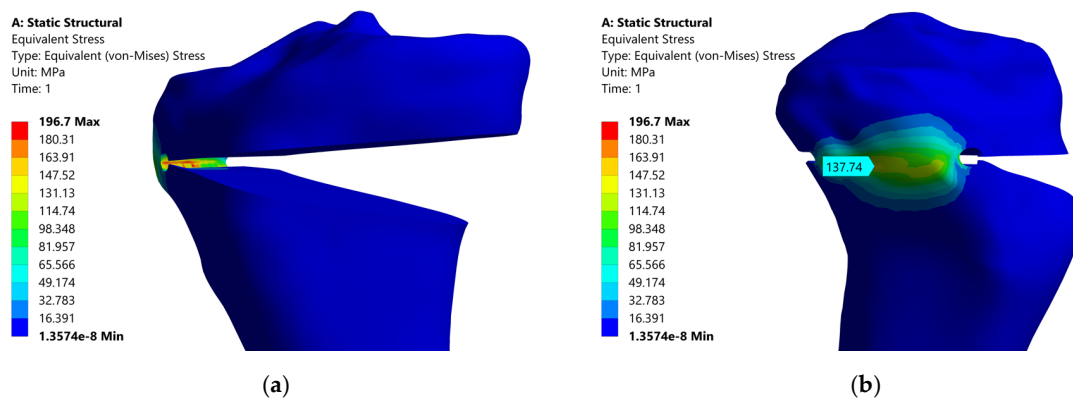


Figure 8. Equivalent von Mises stress in the CORA area—for $X_1 = 30$ mm, $X_2 = 14$ degrees, the inner surface (a) and the outer surface (b).

The FEM analyses were performed similarly for the other previously indicated eight combinations of values, and the results are summarized in Table 2, where the maximum values are presented for both the equivalent von Mises stresses and for the maximum principal stresses.

An increase in the values of these stresses could be noticed with the increase of the correction angle, a trend that is normal. Regarding the other variable, we noticed that the lowest values were recorded for the 40 mm value of the variable X_1 .

An important conclusion is that positioning the cutting point at 40 mm from the intra-articular plane generated the lowest stresses in the CORA area.

Figure 9a–d shows the distribution of the von Mises stresses in the CORA area, both on the inner and on the outer surface of the bone, for the other two scenarios regarding the position of the cutting point (40 mm, 50 mm distance to the tibial plateau) and for the same correction angle of 14 degrees.

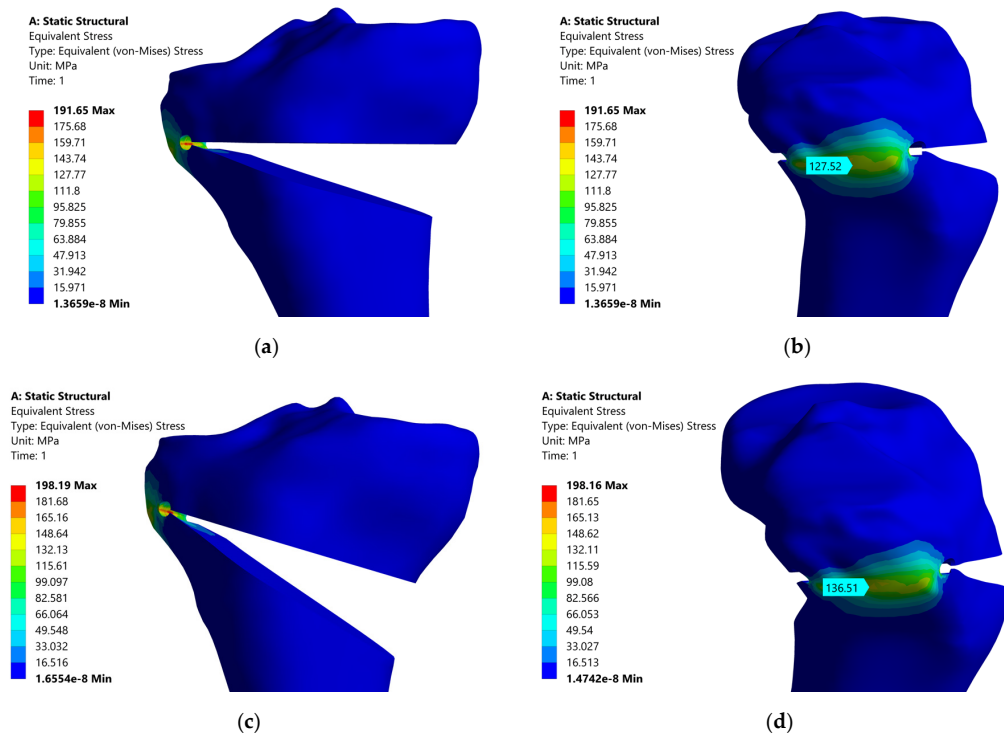


Figure 9. Equivalent von Mises stress in the CORA area—for $X_1 = 40$ mm, $X_2 = 14$ degrees, the inner surface (a) and the outer surface (b) and for $X_1 = 50$ mm, $X_2 = 14$ degrees the inner surface (c) and the outer surface (d).

Another important evaluation made was the comparative analysis of the von Mises stresses on the inner and the outer surfaces of the CORA area for all the three positions of the cutting point (30 mm, 40 mm, 50 mm) in the case of the highest correction angle, namely 14 degrees.

As can be observed in Figure 9, the maximum value of the von Mises stress on the outer wall of the tibia is 127.52 Mpa for the value $X_1 = 40$ mm and 136.51 Mpa for the value $X_1 = 50$ mm. By determining what the difference was between the maximal values of the von Mises stresses inside the CORA area (Table 2) and the stresses from the outer wall of the tibia in the same area, we could also observe the manner in which the stresses propagated in the CORA area. In this sense, for the combination $X_1 = 40$ mm, $X_2 = 14$ degrees, we had the smallest value of the stress on the outer wall—127.52 Mpa—but also the biggest difference between the stresses on the inner and on the outer surfaces (64.13 MPa), from which resulted a smaller speed of propagation of the microfractures.

For the other two combinations, the obtained values were somewhat similar in the sense that the main tension on the outer wall was 137.74 Mpa for $X_1 = 30$ mm, $X_2 = 14$ degrees and 136.51 Mpa for $X_1 = 50$ mm, $X_2 = 14$ degrees, and with respect to the differences between the stresses, these were 58.87 Mpa in the first scenario and 61.65 in the second scenario.

It is therefore recommended to set the initiation cutting point at a 40 mm distance to the tibial plateau. Regarding the other two positions, the 50 mm is slightly better than the 30 mm one.

3.2. Experimental Results Regarding the Study of the Intraoperative Behavior of the Bone Structure in the Case of Opening Tibial Osteotomies

A first output variable studied experimentally during the test was, as previously mentioned, the maximum force F_{\max} measured during the performing of the osteotomy wedge at the required correction angle.

The experimental data were collected in the order in which the tests—the order determined when the experimental program was planned—were conducted. The data are listed in a table and illustrated in self explanatory diagrams. Table 3 shows the values of the maximum forces for the nine combinations of the values of the two variables.

Table 3. Measured values of the maximum force F_{\max} .

| No. | X_1 (mm) | X_2 (Degrees) | F_{\max} (N) |
|-----|------------|-----------------|----------------|
| 1 | 30 | 6 | 419.774 |
| 2 | 30 | 10 | 624.373 |
| 3 | 30 | 14 | 660.231 |
| 4 | 40 | 6 | 241.172 |
| 5 | 40 | 10 | 602.558 |
| 6 | 40 | 14 | 782.012 |
| 7 | 50 | 6 | 367.227 |
| 8 | 50 | 10 | 555.678 |
| 9 | 50 | 14 | 577.410 |

By analyzing the above values, we observed that the absolute maximum of the maximum forces, at which the system yields, was the case of the variable combination: $X_1 = 40$ mm and $X_2 = 14$ degrees. The value of this force was 782.012 N. The minimum value of the maximum force was recorded for the combination: $X_1 = 40$ mm and $X_2 = 6$ degrees.

In order to highlight the variation of the maximum force in relation to each influencing factor, the diagrams shown in Figures 10 and 11 were created.

By analyzing the variation of the maximum force in relation to the correction angle (Figure 10), it could be observed that, at the 40 mm value of the initiation point of the cutting plane, the system withstood the highest force in the case of the 14 degree correction angle, while it recorded the lowest maximum force in the case of the 6 degree angle. At the average value of the angle—10 degrees—the maximum force increased towards the average of the two extremes. The other two curves corresponding

to the values of 30 mm and 50 mm of the cutting point were approximately parallel with the maximum force, recording higher values in the case of the 30 mm value.

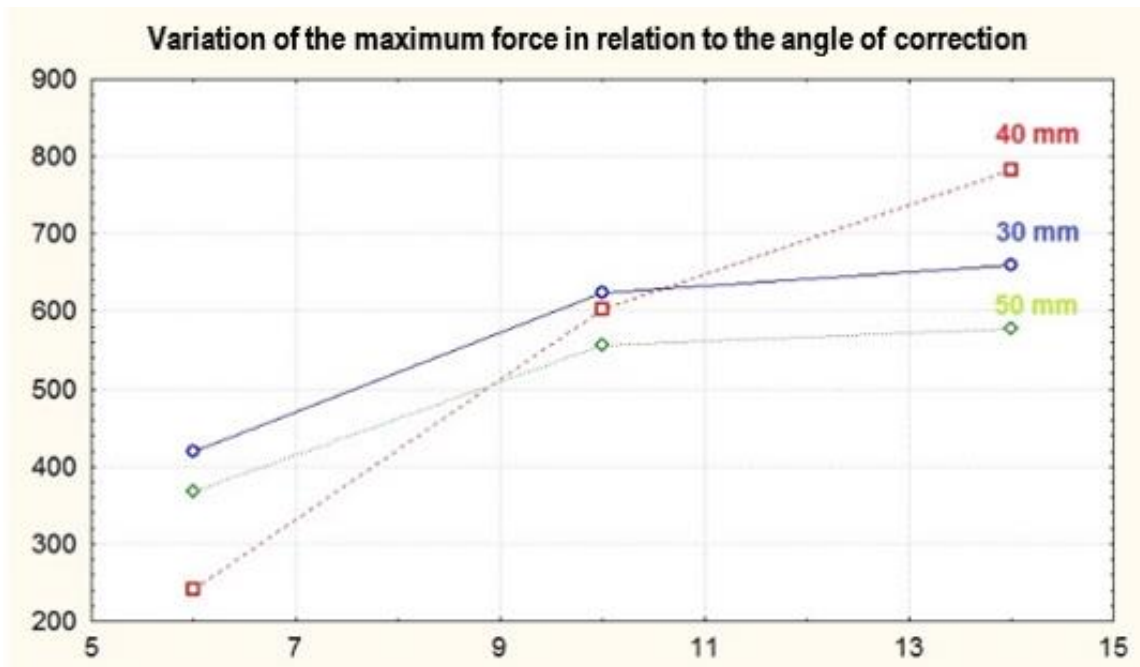


Figure 10. Variation of the maximum force in relation to the correction angle.

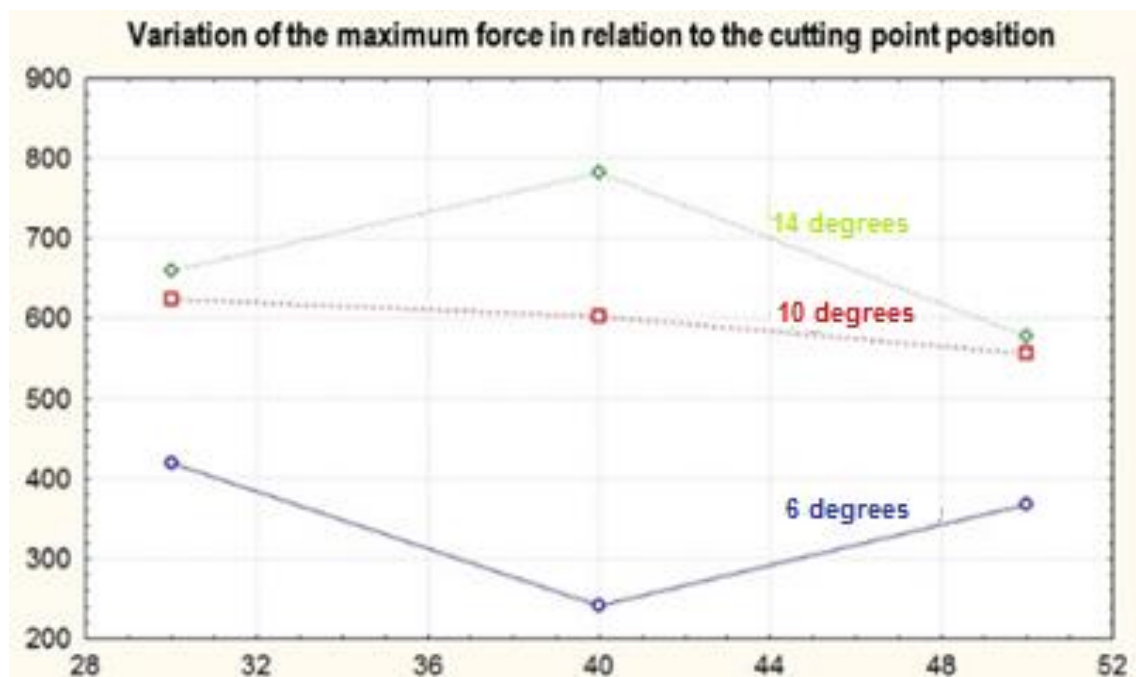


Figure 11. Variation of the maximum force in relation to the position of the cutting point.

The variation in Figure 11 is somewhat natural, considering that the achievement of a higher correction angle requires a greater loading force. We also noticed the close values of the maximum forces in the cases of the 10 degree and the 14 degree correction angles at the 30 and the 50 mm values of the variable, respectively. Obviously, in order to achieve a correction angle of 6 degrees, the values of the maximum forces would be considerably lower.

Another important assessment made during the experiment was the continuous variation of force F related to the displacement (Figure 12). It is interesting to observe the position in which the CORA hinge yields, meaning when the first cracks or microcracks appear, which is an identifiable position when the load suddenly decreases. At a first analysis of the three graphs, it can be seen that the cracking of the CORA area occurred around displacements of about 10 mm when the cutting point was positioned at 30 and 50 mm and at about 15 mm when it was positioned at 40 mm.

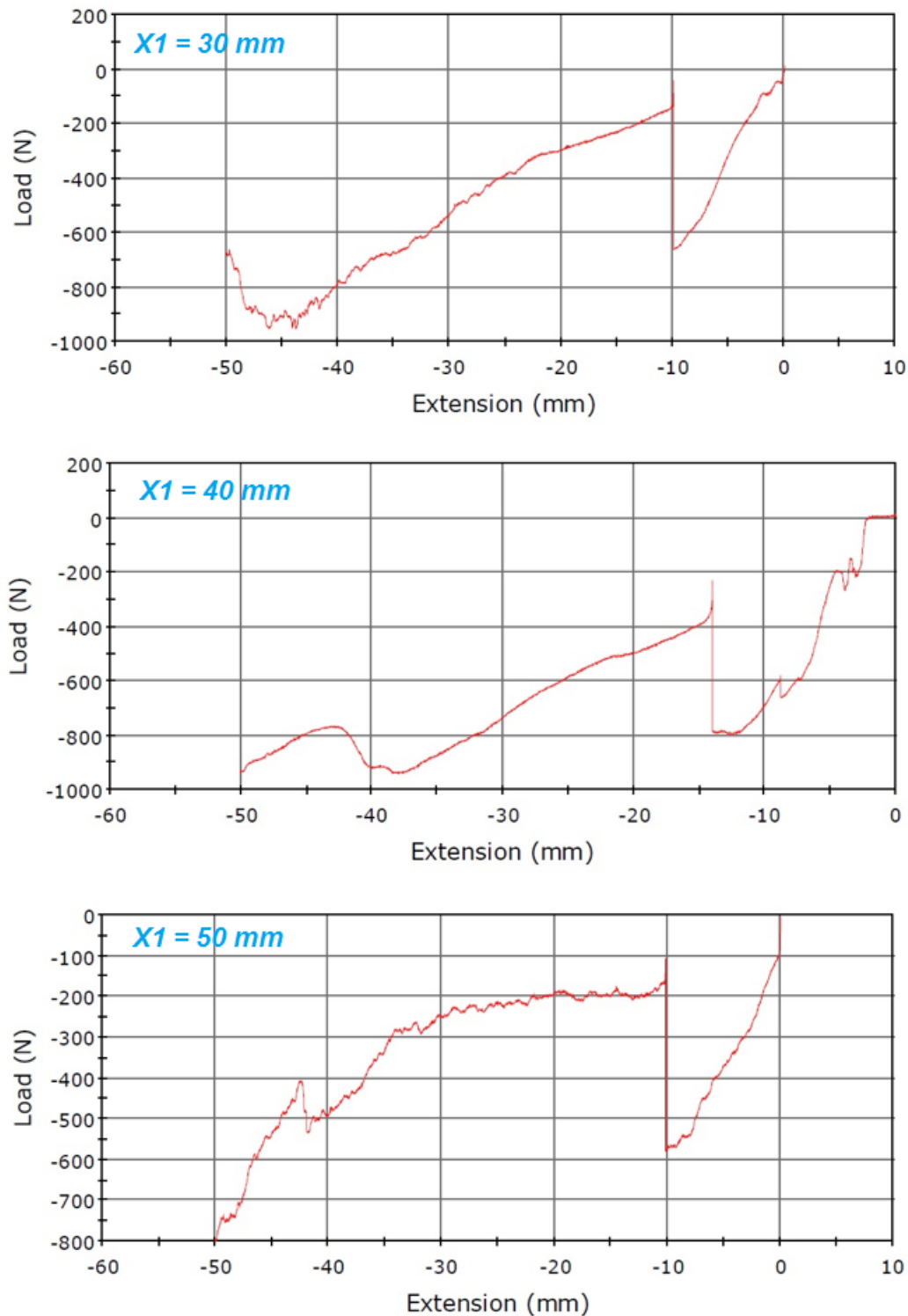


Figure 12. Variation of force relative to the displacement.

In the case of the specimen of tibia where the cutting point was positioned at 30 mm from the tibial plateau, the force reached a maximum of 660.231 N at a displacement of 9.89 mm. It should be noted that, in this case, the system yielded before a correction angle of 14 degrees was achieved, the maximum achievable value being about 11 to 12 degrees, which was still a considerable correction. Proceeding with stressing the tibia up to a displacement of 50 mm, a displacement imposed in all cases, there was a sudden decrease of the force to a value of about 180 N, after which the force increased again, reaching an absolute maximum of 947.534 N at a displacement of 46.1826 mm. During this period, the cracks continued to accumulate until the maximum value was reached.

When the cutting point was positioned at 40 mm from the tibial plateau, the values of the force slightly oscillated at a displacement of 3 to 4 mm. The increase was noticeable and continuous, reaching a maximum of 782.012 N, corresponding to a displacement of 12 mm and implicitly to a correction angle of 14 degrees. It is noteworthy that this was the only situation in which the system did not yield until a correction angle of 14 degrees was achieved, and the graph shows that even larger corrections would be possible, reaching values of about 16 to 18 degrees. At further stressing, up to a displacement of 50 mm, there was a sudden decrease of the force to a value of about 380 N, after which the force increased smoothly, reaching an absolute maximum of 935.678 N.

Finally, for the last presented variation, the one in which the cutting point was positioned at 50 mm from the tibial plateau, the curve was very similar to the one corresponding to the scenario in which the cutting point was positioned at 30 mm in both recorded values and the shape of the variation. An increase in force was observed with a maximum of 577.41 N at a displacement of 10.08 mm. At this point, the system yielded, with a sharp decline of the force valued to 110–120 N. The value remained constant for another 15 mm of displacement, after which it increased at 43 mm, followed by another sudden decrease of about 100 N. The system did not resist until a correction angle of 14 degrees was reached, the maximum achievable value being, again, 11 to 12 degrees. The further application of stress until achieving a displacement of 50 mm resulted in an absolute maximum of 796.470 N, reached at a 49.946 mm displacement.

4. Discussion

This research contributes to the optimization of the geometric planning of the medial open wedge HTO and of other types of surgery. This is illustrated by the results obtained for the two studied variables— X_1 , the position of the cutting point and X_2 , the required angle of correction—by using the two presented research methods, the numerical and the experimental one.

Among the studied parameters, the value of X_2 resulted from the actual axial deviation, whereas the value of X_1 could be appropriately chosen by the surgeon.

We want to note that our research focuses on analyzing the intraoperative behavior of the CORA area and, more specifically, on determining the best combination of parameters (α angle and positioning of the cutting point) for ensuring the success of the surgery and for limiting the appearance of microcracks in the CORA area.

With respect to the FEM study, the sought finality was that of determining the combination of parameters for which there are the lowest stresses in the CORA area.

The values of the von Mises stresses for all the afore mentioned combinations are presented in Figure 13a–c.

It can be observed that, for small correction angles, e.g., 6 degrees, there were only minor differences between the values of the von Mises stresses. The lowest value of the von Mises stress was recorded for the scenario in which the cutting point was positioned at 40 mm. The value registered for the 30 mm scenario was also a convenient one, as the difference in stresses in the two scenarios (40 mm and 30 mm, respectively) was only 1.965 MPa.

For the 10 degree correction angle, the values of the von Mises stresses increased as the value at which the cutting point was positioned increased. Hence, the lowest stress was recorded for the

30 mm position, whereas the highest stress was recorded for the 50 mm position. This made the 50 mm position the least recommended one.

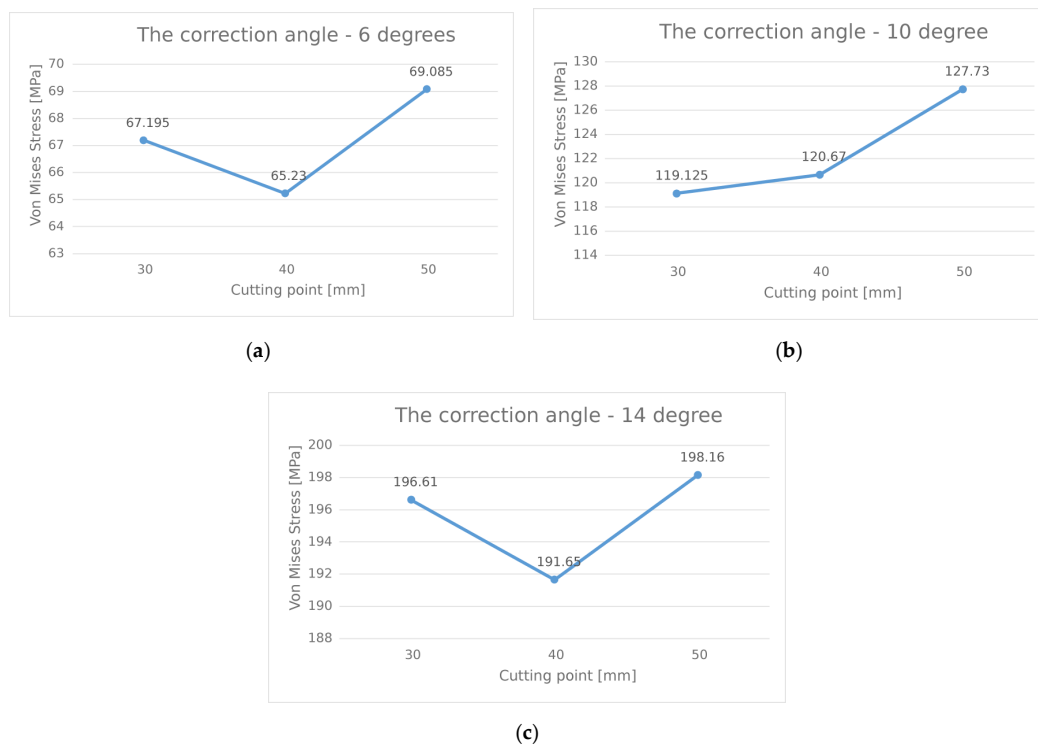


Figure 13. Variation of von Mises stresses in relation to the position of the cutting point. (a) 6 degree; (b) 10 degree; (c) 14 degree.

For higher correction angles, as was the case for the 14 degree correction angle, it was obvious that it was more favorable to position the cutting point at 40 mm, as higher stress values were recorded in the other two scenarios.

In the experimental study, the correction angulation was achieved for the three positions of the cutting point (30 mm, 40 mm, 50 mm). For this approach, the optimal value of the combination of parameters was dependent on the highest obtained value of the maximum force, i.e., the force for which the first microcracks appeared in the CORA area.

Even if, for the experimental research, bovine bones specimens were used, we consider our approach adequate, as it is known that the juvenile bovine bones are frequently used in biomechanical studies because their behavior is highly similar to human bones. In this sense, in article [44], it is confirmed that the long juvenile bovine bones are good study models for the long human bones both from a geometrical and a dimensional point of view, and also with respect to their mechanical characteristics. For example, in accordance to the mentioned study, bone density of the juvenile bovine tibias has values (in the cortical area) of $1.83\text{--}1.96\text{ gcm}^{-3}$, a range that falls inside the density range of the human tibia, as well as the same screw insertion torque and pullout strength. In another article [45], it has been noted that it is appropriate to use bovine bones in biomechanical experiments, the authors highlighting in this sense the ratios between the longitudinal strength of the bovine bone and that of the human bone (1.5–1), respectively between the fracture toughness of the bovine bone and that of the human bone (1.08 to 1.66). Taking into account the fact that the appearance of cracks was the criterion used to determine the optimal combination of parameters, we consider that the obtained results have a high degree of applicability for the purposes of our study.

Further on, we note that bovine bones have also been used for experiments performed in biomechanical studies relating to human bones in papers [46–50].

Reverting to our analysis, as resulted from Figure 11, for the 6 degree angle, the highest value of the maximum force was obtained in the scenario in which the cutting point was positioned at 30 mm, followed by the force obtained in the scenario in which the cutting point was positioned at 50 mm, whereas the least favorable value was that of 40 mm.

For the 10 degree angle, it was for the best to position the cutting point at 30 mm, followed by the 40 mm position and, finally, the 50 mm position.

With respect to the 14 degree angle, it was clearly observed that, by far, the most favorable solution was that of positioning the cutting point at 40 mm, followed by the 30 mm and, finally, the 50 mm scenarios.

From the two used methods, the following joint conclusions result:

- For the 14 degree angle (for high correction values), it was clearly favorable to position the cutting point at 40 mm;
- For the 10 degree angle (for medium correction values), it was favorable to position the cutting point at 30 mm;
- Positioning the cutting point at 50 mm appeared as the least favorable solution for almost all of the used combinations of parameters.

We note that, for the 6 degree angle (for low correction angles), there was a small difference between the two sets of results that we obtained in the sense that FEM recommends positioning the cutting point at 40 mm as favorable, whereas the experimental method recommends positioning it at 30 mm. Considering that the difference in values was small in the case of FEM (the stresses having similar values) and large in the case of the experimental method (the value of the force being considerably higher in the 30 mm scenario), we consider that it is more favorable to position the cutting point at 30 mm.

We consider that the entire studied issue and the obtained results create good premises for the development of future research. An important direction in this sense relates to continuing the study of the intraoperative behavior of the CORA area by taking into account other elements significant for the success of the surgery, such as the importance of executing the relief hole in the CORA hinge area and studying it from a dimensional point of view as well as pursuing and adding to the concerns that exist in this field in literature [28,51–57].

5. Conclusions

The main findings of this study consist in providing concrete information regarding the geometrical and the dimensional planning of the medial wedge open HTO. In order to obtain such information, numerical simulations and an experimental study were performed. The results of this study suggest that, for small correction angles, the optimal position of the cutting point is at 30 mm, while for correction angles of 14 degrees or more, the optimal position of the cutting point is at 40 mm. The obtained values can be applied by interpolation for other values as well, e.g., in the 6–14 degrees range, of the correction angle.

No animal or human studies were carried out by the authors for this article.

Author Contributions: Conceptualization, N.F.C., M.D.R., I.I.C., V.S.O. and S.R.F.; methodology, N.F.C., I.I.C. and V.S.O.; software, N.F.C., I.I.C. and V.S.O.; validation, N.F.C., M.D.R., I.I.C., V.S.O. and S.R.F.; formal analysis, N.F.C.; investigation, N.F.C., M.D.R., V.S.O. and S.R.F.; resources, N.F.C., M.D.R., I.I.C., V.S.O. and S.R.F.; data curation, N.F.C., I.I.C. and V.S.O.; writing—original draft preparation, N.F.C., I.I.C. and V.S.O.; writing—review and editing, N.F.C., M.D.R., I.I.C., V.S.O. and S.R.F.; visualization, N.F.C. and V.S.O.; supervision, N.F.C., V.S.O. and S.R.F.; project administration, N.F.C. All authors have read and agreed to the published version of the manuscript. Authorship must be limited to those who have contributed substantially to the work reported.

Funding: This research received no external funding.

Acknowledgments: Project financed from Lucian Blaga University of Sibiu, The Research centre for sustainable products and processes and Hasso Plattner Foundation research action LBUS-RRC-2020-01.

Conflicts of Interest: The authors declare no conflict of interest.

References

1. Fleaca, R.S. Transplantul Osteocondral Autolog în Tratamentul Leziunilor Cartilajului Articular. Ph.D. Thesis, Lucian Blaga University of Sibiu, Sibiu, Romania, December 2009.
2. Eckstein, F.; Adam, C.; Sittek, H.; Becker, C.; Milz, S.; Schulte, E.; Reiser, M.; Putz, R. Non-invasive determination of cartilage thickness throughout joint surfaces using magnetic resonance imaging. *J. Biomech.* **1997**, *30*, 285–289. [[CrossRef](#)]
3. Eckstein, F.; Winzheimer, M.; Westhoff, J.; Schnier, M.; Haubner, M.; Englmeier, K.H.; Reiser, M.; Putz, R. Quantitative relationships of normal cartilage volumes of the human knee joint—Assessment by magnetic resonance imaging. *Anat. Embryol.* **1998**, *197*, 383–390. [[CrossRef](#)]
4. Potter, H.G.; Foo, L.F. Magnetic Resonance Imaging of Articular Cartilage: Trauma, Degeneration, and Repair. *Am. J. Sports Med.* **2006**, *34*, 661–677. [[CrossRef](#)] [[PubMed](#)]
5. Helminen, H.J.; Kiviranta, I.; Säämänen, A.M.; Jurvelin, J.; Arokoski, J.; Oettmeier, R.; Abendroth, K.; Roth, A.J.; Tammi, M. Effect of motion and load on articular cartilage in animal models. In *Articular Cartilage and Osteoarthritis*; Keuttner, K.E., Schleyerbach, R., Peyron, J.G., Eds.; Raven Press: New York, NY, USA, 1992; pp. 501–510.
6. Abramson, S.B. The role of COX-2 produced by cartilage in arthritis. *Osteoarthr. Cartil.* **1999**, *7*, 380–381. [[CrossRef](#)]
7. Antonescu, D.M.; Pop, D.M. *Elemente de Patologie Osteoarticulara*; Teora Publisher: Bucharest, Romania, 2000; pp. 7–9.
8. Brockmeier, P. Effects of Articular Cartilage Defect Size and Shape on Subchondral Bone Contact: Implications for Surgical Cartilage Restoration. Ph.D. Thesis, The Ohio State University, Athens, OH, USA, June 2008.
9. Derek, T.; Cooke, V.; Allan Scudamore, R.A.; Bryant, T. Mechanical Factors in the Pathogenesis of Osteoarthritis. In *Trends in Research and Treatment of Joint Diseases*; Springer Science and Business Media LLC: Tokyo, Japan, 1992; pp. 29–34.
10. Guilak, F. Biomechanical factors in osteoarthritis. *Best Pr. Res. Clin. Rheumatol.* **2011**, *25*, 815–823. [[CrossRef](#)]
11. Mansur, H.; Rocha, F.A.; Texeira de Dousa Filho, P.G.; De Castro Junior, I.M. Relationship between the knee and hindfoot axes in patients with severe knee osteoarthritis. *Acta Ortop. Bras.* **2020**, *28*, 229–232. [[CrossRef](#)]
12. Amis, A.A. Biomechanics of high tibial osteotomy. *Knee Surg. Sports Traumatol. Arthrosc.* **2013**, *21*, 197–205. [[CrossRef](#)]
13. Floerkemeier, S.; Staubli, A.E.; Schroeter, S.; Goldhahn, S.; Lobenhoffer, P. Outcome after high tibial open-wedge osteotomy: A retrospective evaluation of 533 patients. *Knee Surg. Sports. Traumatol. Arthrosc.* **2013**, *21*, 170–180. [[CrossRef](#)]
14. Ryohei, T.; Hiroyuki, I.; Masato, A.; Haruhiko, B.; Izumi, S.; Ken, K. Medial opening wedge high tibial osteotomy with early full weight bearing. *J. Arthrosc. Relat. Surg.* **2009**, *25*, 46–53. [[CrossRef](#)]
15. Spahn, G. Complications in high tibial (medial opening wedge) osteotomy. *Arch. Orthop. Trauma Surg.* **2003**, *124*, 649–653. [[CrossRef](#)]
16. Sprenger, T.R.; Doerzbacher, J.F. Tibial osteotomy for the treatment of varus gonarthrosis. Survival and failure analysis to twenty-two years. *J. Bone Jt. Surg. Am.* **2003**, *85*, 469–474. [[CrossRef](#)]
17. Amendola, A.; Bonasia, D.E. Results of high tibial osteotomy: Review of the literature. *Int. Orthop.* **2010**, *34*, 155–160. [[CrossRef](#)]
18. Song, E.K.; Seon, J.K.; Park, S.J.; Jeong, M.S. The complications of high tibial osteotomy: Closing- versus opening-wedge methods. *J. Bone Jt. Surg. Br.* **2010**, *92*, 1245–1252. [[CrossRef](#)]
19. Tomofix Medial High Tibial Plate for Medial Tibial Osteotomy. Available online: http://synthes.vo.llnwd.net/o16/LLNWMB8/INT%20Mobile/Synthes%20International/Product%20Support%20Material/legacy_Synthes_PDF/DSEM-TRM-0115-0288-1_LR.pdf (accessed on 15 August 2020).
20. Elson, D.W.; Petheram, T.G.; Dawson, M.J. High reliability in digital planning of medial opening wedge high tibial osteotomy, using Miniaci's method. *Knee. Surg. Sports Traumatol. Arthrosc.* **2015**, *23*, 2041–2048. [[CrossRef](#)]
21. Modern High Tibial Osteotomy. Available online: <http://www.ilizarov.org/HTO1.pdf> (accessed on 15 August 2020).
22. Yin, Y.; Li, S.; Zhang, R.; Guo, J.; Hou, Z.; Zhang, Y. What is the relationship between the “Fujisawa point” and postoperative knee valgus angle? A theoretical, computer-based study. *Knee* **2020**, *27*, 183–191. [[CrossRef](#)]

23. Somtua, C.; Aroonjarattham, P.; Aroonjarattham, K. The correction of Thai varus knee by high tibial osteotomy with Fujisawa's point using finite element analysis. *J. Res. Appl. Mech. Eng.* **2019**, *7*, 45–59.
24. Yang, J.C.; Chen, C.F.; Luo, C.A.; Chang, M.C.; Lee, O.K.; Huang, Y.; Lin, S.C. Clinical Experience Using a 3D-Printed Patient-Specific Instrument for Medial Opening Wedge High Tibial Osteotomy. *BioMed Res. Int.* **2018**, *2018*, 1–9. [CrossRef]
25. Rudzki, J.R. Medial Opening Wedge High Tibial Osteotomy, Arthrex Knee Meeting, Los Angeles, CA, USA, 12 May 2012. Published on 23 January 2015. Available online: <https://www.slideshare.net/washingtonortho/arthrex-hto-talk-51212> (accessed on 20 November 2020).
26. Kader, D. High Tibial Osteotomy and UniKnee, Health & Medicine. 2015. Available online: <https://www.slideshare.net/ProfDeiaryFKader/high-tibial-osteotomy-and-uniknee-for-post-grad-orth-frcs-course> (accessed on 20 November 2020).
27. Lee, Y.S.; Moon, G.H. Comparative analysis of osteotomy accuracy between the conventional and devised technique using a protective cutting system in medial open-wedge high tibial osteotomy. *J. Orthop. Sci.* **2015**, *20*, 129–136. [CrossRef]
28. Kwun, J.D.; Kim, H.J.; Park, J.; Park, I.H.; Kyung, H.S. Open wedge high tibial osteotomy using three-dimensional printed models: Experimental analysis using porcine bone. *Knee* **2017**, *24*, 16–22. [CrossRef]
29. Ogawa, H.; Matsumoto, K.; Akiyama, H. The prevention of a lateral hinge fracture as a complication of a medial opening wedge high tibial osteotomy—a case control study. *Bone Jt. J.* **2017**, *99*. [CrossRef]
30. Ionescu, I.; Conway, T.; Schonning, A.; Almutairi, M.; Nicholson, D.W. Solid Modeling and Static Finite Element Analysis of the Human Tibia. In Proceedings of the Summer Bioengineering Conference 2003, Sonesta Beach Resort, Key Biscayne, FL, USA, 25–29 June 2003.
31. Isaksson, H.E. Mechanical and Mechanobiological Influences on Bone Fracture Repair: Identifying Important Cellular Characteristics. Ph.D. Thesis, Eindhoven University of Technology, Eindhoven, The Netherlands, November 2007. [CrossRef]
32. Cilingira, A.C.; Ucara, V.; Kazana, R. Three-Dimensional Anatomic Finite Element Modelling of Hemi-Arthroplasty of Human Hip Joint. *Trends Biomater. Artif. Organs* **2007**, *21*, 63–72.
33. Petersen, W.; Zantop, T. Anatomy of the anterior cruciate ligament with regard to its two bundles. *Clin. Orthop. Relat.* **2007**, *454*, 35–47. [CrossRef] [PubMed]
34. Müller-Karger, C.; Larrazabal, C.A. Finite Element Bone Model Incorporating Heterogeneity and Anisotropy from CT. In Proceedings of the ISB XXth Congress of the International Society of Biomechanics and ASB 29th Annual Meeting of the American Society of Biomechanics, Cleveland, OH, USA, 31 July–5 August 2004.
35. Galik, K. The Effect of Design Variations on Stresses in Total Ankle Arthroplasty. Ph.D. Thesis, University of Pittsburgh, Pittsburgh, PA, USA, April 2002.
36. Bayraktara, H.H.; Morgana, E.F.; Nieburb, G.L.; Morrissa, G.E.; Wonga, E.K.; Keaveny, T.M. Comparison of the elastic and yield properties of human femoral trabecular and cortical bone tissue. *J. Biomech.* **2004**, *37*, 27–35. [CrossRef]
37. Kelly, D.J.; Predengast, P.J. Prediction of the Optimal Mechanical Properties for a Scaffold Used in Osteochondral Defect Repair. *Tissue Eng.* **2006**, *12*, 2509–2519. [CrossRef] [PubMed]
38. Yao, J.; Salo, A.D.; Barbu-Mcinnis, M.; Lerner, A.L. Finite Element Modeling of Knee Joint Contact Pressures and Comparison to Magnetic Resonance Imaging of the Loaded Knee. In Proceedings of the IMECE'032003 ASME International Mechanical Engineering Congress & Exposition, Washington, DC, USA, 16–21 November 2003.
39. Boruah, S.; Subit, D.L.; Paskoff, G.R.; Shender, B.S.; Crandall, J.R.; Salzar, R.S. Influence of bone microstructure on the mechanical properties of skull cortical bone—A combined experimental and computational approach. *J. Mech. Behav. Biomed. Mater.* **2017**, *65*, 688–704. [CrossRef]
40. Leordean, D.; Dudescu, C.; Marcu, T.; Berce, P.; Balc, N. Customized implants with specific properties, made by selective laser melting. *Rapid Prototyp. J.* **2015**, *21*, 98–104. [CrossRef]
41. Cofaru, I.I. Research on the Biomechanics of Axial Deviations of the Human Lower Limb and the Development of Related Surgical Equipment. Ph.D. Thesis, Lucian Blaga University of Sibiu, Sibiu, Romania, November 2013.
42. Morgan, F.; Bayraktar, H.H.; Keaveny, T.M. Trabecular bone modulus–density relationships depend on anatomic site. *J. Biomech.* **2003**, *36*, 897–904. [CrossRef]

43. Koh, Y.G.; Lee, J.A.; Lee, H.Y.; Chun, H.J.; Kim, H.J.; Kang, K.T. Design optimization of high tibial osteotomy plates using finite element analysis for improved biomechanical effect. *J. Orthop. Surg. Res.* **2019**, *14*, 1–10. [[CrossRef](#)]
44. Fletcher, J.W.A.; Williams, S.; Whitehouse, M.R.; Gill, H.S.; Preatoni, E. Juvenile bovine bone is an appropriate surrogate for normal and reduced density human bone in biomechanical testing: A validation study. *Sci. Rep.* **2018**, *8*, 1–9. [[CrossRef](#)]
45. Sisljagic, V.; Jovanovic, S.; Mrcela, T.; Nikolic, V.; Radic, R.; Wertheimer, V.; Tanja Kovac, T.; Mrcela, M. Applicability of bovine tibia as a model in research on various osteosynthesis techniques. *Period. Biol. UDC* **2010**, *112*, 59–62.
46. Bowland, P.; Cowie, R.M.; Ingham, E.; Fisher, J.; Jennings, M. Biomechanical assessment of the stability of osteochondral grafts implanted in porcine and bovine femoral condyles. *Proc. Inst. Mech. Eng. Part H. J. Eng. Med.* **2019**, *234*, 163–170. [[CrossRef](#)]
47. Akhbar, M.F.A.; Yuosoff, A.R. Comparison of bone temperature elevation in drilling of human, bovine and porcine bone. *Sci. Direct* **2019**, *82*, 411–414. [[CrossRef](#)]
48. Hillerya, M.T.; Shuaibb, I. Temperature effects in the drilling of human and bovine bone. *J. Mater. Process. Technol.* **1999**, 302–308. [[CrossRef](#)]
49. Brown, C.P.; Nguyen, T.C.; Moody, H.R.; Crawford, R.W.; Oloyede, A. Assessment of common hyperelastic constitutive equations for describing normal and osteoarthritic articular cartilage. *Proc. Inst. Mech. Eng. Part H-J. Eng. Med.* **2009**, *223*, 643–652. [[CrossRef](#)] [[PubMed](#)]
50. Demarteau, O.; Pillet, L.; Inaebnit, A.; Borens, O.; Quinn, T.M. Biomechanical characterization and in vitro mechanical injury of elderly human femoral head cartilage: Comparison to adult bovine humeral head cartilage. *Osteoarthr. Cartil.* **2006**, *14*, 589–596. [[CrossRef](#)]
51. Koh, Y.G.; Son, J.; Kim, H.J.; Kwon, S.K.; Kwon, O.R.; Kim, H.J.; Kang, K.T. Multi-objective design optimization of high tibial osteotomy for improvement of biomechanical effect by using finite element analysis. *J. Orthop. Res.* **2018**, *36*, 2956–2965. [[CrossRef](#)]
52. Russu, O.M.; Strnad, G.; Farkas, L.J.; Cazacu, R.; Feier, A.; Gergely, I.; Trambitas, C.; Petrovan, C. Electrochemical Synthesis of Nanostructured Oxide Layers on Threaded Surfaces of Medical Implants. *Rev. Chim.* **2018**, *69*, 1636–1639. [[CrossRef](#)]
53. Andor, B.; Patrascu, J.M.; Florescu, S.; Cojocar, D.; Sandesc, M.; Borcan, F.; Boruga, O.; Bolinteanu, S. Comparison of Different Knee Implants Used on Patients with Osteoarthritis Control Study. *Mater. Plast.* **2016**, *53*, 119–125.
54. Todor, A.; Vermesan, D.; Haragus, H., Jr.; Patrascu, J.M.; Timar, B.; Cosma, D.I. Cross-cultural adaptation and validation of the Romanian International Knee Documentation Committee—Subjective knee form. *PeerJ.* **2020**, *8*, e8448. [[CrossRef](#)]
55. Csernátó, Z.; Kiss, L.; Manó, S. A new technique of wedge osteotomy to diminish undesirable fractures. *Eur. J. Orthop. Surg. Traumatol.* **2008**, *18*, 485–488. [[CrossRef](#)]
56. Chernchujit, B.; Tharakulphan, S.; Prasertia, R.; Chantarapanich, N.; Jirawison, C.; Sitthiseripratip, K. Preoperative planning of medial opening wedge high tibial osteotomy using 3D computer-aided design weight-bearing simulated guidance: Technique and preliminary result. *J. Orthop. Surg.* **2019**, *27*. [[CrossRef](#)] [[PubMed](#)]
57. Mohamed, E.A. Opening wedge high tibial osteotomy in varus osteoarthritis of the knee without bone graft. *Egypt. Orthop. J.* **2018**, *53*, 38–43. [[CrossRef](#)]

Publisher’s Note: MDPI stays neutral with regard to jurisdictional claims in published maps and institutional affiliations.



© 2020 by the authors. Licensee MDPI, Basel, Switzerland. This article is an open access article distributed under the terms and conditions of the Creative Commons Attribution (CC BY) license (<http://creativecommons.org/licenses/by/4.0/>).